Magnetic phase transitions of insulating spin-orbit coupled Bose atoms in one-dimensional optical lattices

Li Zhang◉, Yongguan Ke, and Chaohong Lee◉[*]

Guangdong Provincial Key Laboratory of Quantum Metrology and Sensing & School of Physics and Astronomy,
Sun Yat-Sen University (Zhuhai Campus), Zhuhai 519082, China
and State Key Laboratory of Optoelectronic Materials and Technologies, Sun Yat-Sen University
(Guangzhou Campus), Guangzhou 510275, China

We consider the insulating spin-orbit coupled Bose atoms confined within one-dimensional optical lattices and explore their ground-state magnetic phase transitions. Under strong interactions, the charge degrees of atoms are frozen and the system can be described by an anisotropic XXZ Heisenberg chain with Dzyaloshinskii-Moriya interaction and transverse field. We apply the matrix product state method to obtain the ground states, and analyze spiral correlation functions, spin-spin correlation functions, and first energy gap. Under weakly transverse fields, the ground state is a ferromagnetic phase if the interspin s-wave interaction strength is stronger than that of the intraspin ones, otherwise, it is a paramagnetic phase, an antiferromagnetic phase, or a gapless spiral phase with algebraic decaying spin correlations. When the transverse field is strengthened, the gapless spiral phase is broken and a new spiral phase with long-range spin-spin correlations emerges.

I. INTRODUCTION

Ultracold spinor atoms in an optical lattice provide an excellent platform for simulating magnetic phase transitions in quantum Heisenberg models. In the Mott regime, the fluctuation of charge degree of spinor atoms is suppressed. The low-energy physics can be captured by an effective spin superexchange model [1–3], where the spin-spin coupling can be tuned via spin-dependent s-wave scattering and lattice depth. In recent years, there was a lot of interest in creating synthetic gauge fields and spin-orbital coupling (SOC) [4–7]. In optical lattice systems, SOC is engineered via dressing an optical lattice with periodic Raman potentials [8–10], or synthesizing a ladderlike system subject to gauge fields by Raman-assisted tunneling [11–14] and optical clock transition [15–17]. In the ladderlike system, the ladder legs are labeled by either the internal spin states or the real-space lattices, which can be mapped to effective spin [18]. In these setups, the SOC induces either nearest-neighbor or on-site spin-flip.

In addition to the realistic atom-atom interaction, the SOC plays a key role in magnetic phase transitions. It may modify the anisotropic couplings and lead to the so-called Dzyaloshinskii-Moriya (DM) exchange interaction [19,20], which induces exotic magnetic phases. In two-dimensional (2D) systems, the coexistence of DM interaction and anisotropic couplings gives rise to spiral phases, vortex crystal structure, and novel Skymion, apart from the normal ferromagnetic and antiferromagnetic phases [21–25]. Classical phase diagrams have been obtained by Monte Carlo simulations [22,24], steepest descent minimization method [23],

and variational mean-field approach [25]. In one-dimensional (1D) systems, the effective model reduces into an anisotropic Heisenberg chain with a one-component DM interaction. The novel phase structures in 2D systems are simplified to a gapless spiral phase on the plane perpendicular to the DM vector, which belongs to the gapless Luttinger liquid (LL) phase [26–28]. The various phases and phase diagrams in 1D systems are widely studied using density matrix renormalization group method [26–30].

Most previous works concentrated on nearest-neighbor spin-flip induced by SOC, where the effective models do not contain any external fields, in particular, on-site spin-flip fields. An XXZ model with DM interaction and transverse field has been realized in a 1D fermionic ladderlike optical lattice with synthetic magnetic flux [31]. The external field provides a new flexible freedom to tune the phase diagram. However, owing to the absence of asymmetric s-wave scattering, this model can be mapped to an isotropic antiferromagnetic XXX spin chain in a spiral field, thus there are only two phases in this model: a gapless LL phase and a fully polarized phase. One can alternately load spinor (two-component) bosons into such a lattice, where the spin-dependent s-wave scattering can cause anisotropic spin-spin couplings. Furthermore, since both fermionic [13,15–17] and bosonic [12] ladders subject to gauge field have been realized in experiments, there is no reason to leave the bosonic case unexplored.

In this article we study the quantum magnetic phase transitions of insulating spin-orbit coupled bosons in a 1D optical lattice. Utilizing the SOC-dressed Hubbard model realized in a recent experiment [12], we derive an effective spin model in the strong repulsive interaction limit: an XXZ model with DM interaction subject to external transverse field. The strength of the anisotropy, DM interaction, and transverse field of the spin

———————
[*]lichaoh2@mail.sysu.edu.cn; chleecn@gmail.com

model can be tuned by the parameters of the optical lattice and the SOC strength. By employing the variational matrix product state (MPS) approach [32–34], we obtain the ground states (GSs) and the energy gap between the GS and the first excited state. Then, by calculating the spiral and spin-spin correlation functions for the GS and the first energy gap, we identify four different phases with ferromagnetic, paramagnetic, antiferromagnetic, and spiral long-range correlations, and give rich phase diagrams in different parameter regions. In particular, in the weak transverse field limit, the spiral phase is a LL with algebraically decaying spin-spin correlations. The strengthened transverse field induces a new spiral phase with long-range spin-spin correlations.

The article structure is as follows. In this section we introduce the related background and our motivation. In Sec. II we derive the effective Hamiltonian for our physical system. In Sec. III we apply the MPS method to study the GS properties and present the corresponding phase diagrams. In the last section we summarize and discuss our results.

II. STRONGLY INTERACTING SPIN-ORBIT COUPLED BOSE ATOMS IN 1D OPTICAL LATTICES

Recent experiments have realized spin-orbit coupled bosons in a 1D optical lattice by coupling the three internal states (pseudospins) with Raman-assisted transition [12]. It is a virtual three-leg ladder pierced by magnetic flux ϕ, where the internal states of the bosons provide the extra dimension. It can be reduced to a two-leg ladder if the second-order Zeeman shift is large enough that the upper internal level can be removed [35]. Moreover, such a bosonic ladder may also be realized by coupling metastable states of Bose atoms by an optical clock transition, which has been utilized to realize a fermionic ladder in a gauge field [15–17]. Here we choose the Landau gauge, where the phase is accumulated by intraleg hopping and a net flux of ϕ is created through each plaquette. The single-particle Hamiltonian of this system is written as

$$\hat{H}_t = -t \sum_j \left(e^{i\frac{\phi}{2}} \hat{a}^\dagger_{j,\uparrow} \hat{a}_{j+1,\uparrow} + e^{-i\frac{\phi}{2}} \hat{a}^\dagger_{j,\downarrow} \hat{a}_{j+1,\downarrow} + \text{H.c.} \right)$$
$$- \frac{\Omega}{2} \sum_j (\hat{a}^\dagger_{j,\uparrow} \hat{a}_{j,\downarrow} + \text{H.c.}), \tag{1}$$

where $\hat{a}^\dagger_{j,\sigma}$ ($\sigma = \uparrow, \downarrow$) creates a particle of internal state (pseudospin) σ at site j. The first term is the spin-conserved nearest-neighbor hopping with strength $te^{\pm i\frac{\phi}{2}}$, where t can be tuned by the depth of the optical lattice, and the magnetic flux ϕ is related to the SOC momentum k_{SOC} by $\phi = k_{\text{SOC}}\pi/k_L$, where k_L is the lattice momentum. The SOC momentum k_{SOC} is the momentum transfer of the Raman lasers and can be tuned by choosing different wavelength and/or changing the relative angle of them [11,12]. The second term describes the on-site spin-flip with strength $\frac{\Omega}{2}$, with Ω being the Rabi frequency of the Raman lasers. Multiple particles in this optical lattice are described by the Hamiltonian $\hat{H} = \hat{H}_t + \hat{H}_U$, with the interaction term

$$\hat{H}_U = \frac{1}{2} \sum_{j,\sigma} U_{\sigma\sigma} \hat{n}_{j\sigma}(\hat{n}_{j\sigma} - 1) + U_{\uparrow\downarrow} \sum_j \hat{n}_{j\uparrow}\hat{n}_{j\downarrow}, \tag{2}$$

where $\hat{n}_{j\sigma} = \hat{a}^\dagger_{j\sigma}\hat{a}_{j\sigma}$ is the particle number operator. The on-site interspin and intraspin interaction strengths are denoted as $U_{\uparrow\downarrow}$ and $U_{\sigma\sigma}$, respectively, which can be tuned by Feshbach resonance. In the following, we set repulsive interaction as $U_{\uparrow\uparrow} = U_{\downarrow\downarrow} = U > 0$ and $U_{\uparrow\downarrow} = \lambda U > 0$.

We are interested in the magnetic properties in the deep Mott insulator regime at half-filling with strong interaction $U, U_{\uparrow\downarrow} \gg t, \Omega$. We employ the perturbation theory for the degenerate quantum system to obtain the effective Hamiltonian [36]. We treat the tunneling Hamiltonian $\hat{H}_t$ as a perturbation to the on-site interaction $\hat{H}_U$. The GS of $\hat{H}_U$ is a Mott insulator with exactly one particle per site. It is many-fold degenerate since the spin on every site is arbitrary. $\hat{H}_t$ couples the manifold ground states of $\hat{H}_U$ via virtual processes. Defining the spin operators $\mathbf{S}_j = \frac{1}{2}\hat{a}^\dagger_{j\alpha}\boldsymbol{\sigma}_{\alpha\beta}\hat{a}_{j\beta}$, where $\boldsymbol{\sigma}$ are the Pauli matrices, the effective Hamiltonian up to second order reads as

$$\hat{H}_{\text{eff}} = J \sum_j \left[\cos\phi \left(\hat{S}^x_j \hat{S}^x_{j+1} + \hat{S}^y_j \hat{S}^y_{j+1} \right) + J_z \hat{S}^z_j \hat{S}^z_{j+1} \right.$$
$$\left. + \mathbf{D} \cdot (\mathbf{S}_j \times \mathbf{S}_{j+1}) \right] - \Omega \sum_j \hat{S}^x_j, \tag{3}$$

where $J = -\frac{4t^2}{\lambda U}$, $J_z = 2\lambda - 1$, and the DM vector $\mathbf{D} = (0, 0, \sin\phi)$ (see Appendix A for details of the derivation). The effective Hamiltonian is an anisotropic XXZ Heisenberg model with DM interaction and transverse field. The Heisenberg coupling and DM interaction proportional to J are induced by flux dependent nearest-neighbor hopping; The transverse field proportional to Ω is induced by the on-site spin-flip.

In the following, we study the ground states of Hamiltonian (3). We restrict our discussion in the regime $\phi \in [0, \pi]$, since it is accessible in the experiments, and Eq. (3) satisfies $\hat{\Gamma}\hat{H}_{\text{eff}}(\phi, \lambda, \Omega)\hat{\Gamma}^\dagger = \hat{H}_{\text{eff}}(-\phi, \lambda, \Omega)$, with $\hat{\Gamma} = \prod_j 2\hat{S}^x_j$ in the theoretical perspective. Besides, we scale the energy by $\frac{4t^2}{U}$ and define $\Omega' = \Omega/\frac{4t^2}{U}$.

III. MAGNETIC PHASE TRANSITIONS

The Hamiltonian (3) for arbitrary parameters (ϕ, λ, Ω') cannot be analytically solved. We apply the MPS method to determine the GS under open boundary condition [32–34], calculate the expectation value of observables and the first energy gap, and then give the corresponding phase diagrams. We show results for a chain with length $L = 195$, unless otherwise specified. The details of our calculation procedure can be found in Appendix B.

For a given GS $|\psi_0\rangle$, one can calculate the spiral correlation functions

$$\mathcal{C}^\alpha_{j,l} = \langle\psi_0|[\mathbf{S}_j \times \mathbf{S}_{j+1}]^\alpha [\mathbf{S}_l \times \mathbf{S}_{l+1}]^\alpha|\psi_0\rangle, \tag{4}$$

and spin-spin correlation functions

$$\mathcal{S}^\alpha_{j,l} = \langle\psi_0|\hat{S}^\alpha_j \hat{S}^\alpha_l|\psi_0\rangle, \tag{5}$$
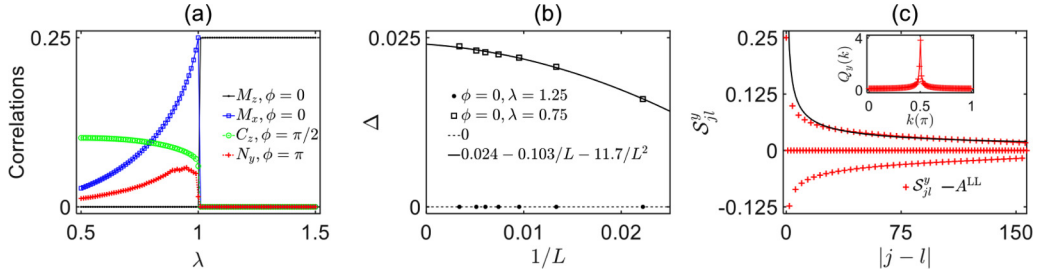
FIG. 1. (a) The long-range correlations versus λ for $\Omega' = 10^{-3}$ and different values of ϕ. M_x and M_z are plotted for $\phi = 0$ (solid blue line marked by squares and black line by dots, respectively); C_z is plotted for $\phi = \pi/2$ (dashed green line marked by circles); and N_y is plotted for $\phi = \pi$ (dotted red line marked by pluses). (b) Finite-size scaling of the first energy gap Δ for the z-FM phase (dashed line with dots) at $(\phi, \lambda, \Omega') = (0, 1.25, 10^{-3})$ and the x-PM phase (solid line with squares) at $(\phi, \lambda, \Omega') = (0, 0.75, 10^{-3})$. The dots and squares are calculated with system size $L = 45, 75, 105, 135, 165, 195,$ and 295. The solid and dashed lines are the fittings. (c) The spin-spin correlation function $\mathcal{S}_{jl}^y$ (red pluses) versus $|j - l|$ for the LL-SP phase, at the parameter point $(\phi, \lambda, \Omega') = (0.5\pi, 0.75, 10^{-3})$. The envelop of $\mathcal{S}_{jl}^y$ is well fitted by the function $A^{\mathrm{LL}}(|j - l|) = 0.33/|j - l|^{0.56}$ (black line). Inset in (c): The spin structure factor $Q_y(k)$ versus k.

where $\alpha = x, y,$ and z. The structure factors associated with $\mathcal{S}_{jl}^\alpha$ read as

$$Q_\alpha(k) = \frac{1}{L} \sum_{jl} e^{ik(j-l)} \mathcal{S}_{j,l}^\alpha, \qquad (6)$$

where L is the system size, and k is the momentum. In order to distinguish different phases, we introduce the long-range spiral correlations

$$C_\alpha = \frac{1}{d+1} \sum_{r=r_0}^{r_0+d} \langle \mathcal{C}_{j,j+r}^\alpha \rangle_j, \qquad (7)$$

the long-range ferromagnetic correlations

$$M_\alpha = \frac{1}{d+1} \sum_{r=r_0}^{r_0+d} \langle \mathcal{S}_{j,j+r}^\alpha \rangle_j, \qquad (8)$$

the long-range Néel correlations

$$N_\alpha = \frac{1}{d+1} \sum_{r=r_0}^{r_0+d} (-1)^r \langle \mathcal{S}_{j,j+r}^\alpha \rangle_j, \qquad (9)$$

where $\langle \cdot \rangle_j$ means averaging over j, and r_0 is chosen as a large distance (in particular, we take $r_0 = 100$ and $d = 49$), and the first energy gap

$$\Delta = E_1 - E_0, \qquad (10)$$

where E_1 and E_0 are the energy of the first excited state and the GS, respectively. Therefore, one can divide the GS into four different phases: (I) the α-FM phase with nonzero M_α and closed first energy gap; (II) the α-PM phase with nonzero M_α and finite first energy gap; (III) the α-AFM phase with nonzero N_α; and the spiral phase with nonzero C_α. Interestingly, we find that there are two kinds of spiral phases in our system: (IV) the LL-SP phase with algebraically decaying spin-spin correlation functions, and (V) the xy-SP phase with finite long-range spin-spin correlations.

Under weak external fields ($\Omega' \ll 1$), when $\lambda > 1$, the GS will be a z-FM phase in (I); when $\lambda < 1$, the GS will be a x-PM phase in (II) for $\phi \approx 0$, a y-AFM phase in (III) for $\phi \approx \pi$, and a LL-SP phase in (IV) otherwise. In Fig. 1(a) we plot M_x and M_z (for $\phi = 0$), C_z and M_z (for $\phi = 0.5\pi$),

and N_y and M_z (for $\phi = \pi$), as functions of λ. We note that the curves for M_z at $\phi = 0.5\pi$ and π overlap with that at $\phi = 0$, so we do not show them further. We observe all the related long-range correlations abruptly change at the critical point $\lambda = 1$. The ferromagnetic phase and the paramagnetic phase are distinguished by the first energy gap Δ, which vanishes for the ferromagnetic phase and retains finite for the paramagnetic phase in the thermodynamic limit, see Fig. 1(b). By extrapolating Δ to infinite system size, $\Delta = 0$ for the z-FM phase at parameter point $(\phi, \lambda, \Omega') = (0, 1.25, 10^{-3})$ and $\Delta = 0.024 - 0.103/L - 11.7/L^2$ for the x-PM phase at parameter point $(\phi, \lambda, \Omega') = (0, 0.75, 10^{-3})$.

The phase transitions under weak external fields can be intuitively interpreted via transforming the Hamiltonian (3) to an XXZ Heisenberg model in a spiral field,

$$\hat{H}'_{\mathrm{eff}} = -\frac{1}{\lambda} \sum_j \left[\hat{S}_j^x \hat{S}_{j+1}^x + \hat{S}_j^y \hat{S}_{j+1}^y + (2\lambda - 1)\hat{S}_j^z \hat{S}_{j+1}^z \right]$$
$$- \Omega' \sum_j \left[\cos(\phi j)\hat{S}_j^x - \sin(\phi j)\hat{S}_j^y \right], \qquad (11)$$

which relates to $\hat{H}_{\mathrm{eff}}$ through the unitary transformation $\hat{H}'_{\mathrm{eff}} = \hat{U}\hat{H}_{\mathrm{eff}}\hat{U}^\dagger$ with $\hat{U} = \prod_j e^{i\phi j \hat{S}_j^z}$. When $\Omega' = 0$, it is a standard ferromagnetic XXZ model, whose GS has been solved exactly by the Bethe ansatz [37]. As a result, when $\lambda > 1$, the GS is in the z-FM phase. When $\lambda < 1$, it is in the gapless LL, with algebraically decaying spin-spin correlation functions. Regarding the original Hamiltonian, the flux ϕ makes the phases more complicated. When $\lambda > 1$, the ground state is in the z-FM phase regardless of any ϕ. When $\lambda < 1$, the gapless LL phase transforms to a gapless ferromagnet on the $\hat{x}\hat{y}$ plane for $\phi = 0$, a gapless antiferromagnet on the $\hat{x}\hat{y}$ plane for $\phi = \pi$, and a gapless spiral phase for $0 < \phi < \pi$. If the external field is slightly turned on, the gapless ferromagnet will be polarized in the $\hat{x}$ direction, and the GS is in the gapped x-PM phase; the gapless antiferromagnet will favor long-range antiferromagnetic order along the $\hat{y}$ direction [38], and the GS is in the twofold degenerate y-AFM phase; however, the gapless spiral phase is not explicitly influenced by the weak external field, still featuring the nature of the LL phase. We calculate the spin-spin correlation functions for the

LL-SP phase, and find that, as expected, $\mathcal{S}_{jl}^x$ and $\mathcal{S}_{jl}^y$ show the same particular behavior. That is, they oscillate as functions of $|j - l|$ at a period of nearly $2\pi/\phi$ sites, and the envelopes decay algebraically. This behavior is well fitted by

$$f^{\mathrm{LL}}(|j - l|) = A^{\mathrm{LL}}(|j - l|) \cos(2\pi|j - l|/\phi), \qquad (12)$$

where the envelope satisfies

$$A^{\mathrm{LL}}(|j - l|) = a/|j - l|^p. \qquad (13)$$

The fitting parameters a and p are dependent on ϕ, λ, and Ω'. In Fig. 1(c) we plot $\mathcal{S}_{jl}^y$ and the structure factor $Q_y(k)$ for the LL-SP phase at a representative parameter point $(\phi, \lambda, \Omega') = (0.5\pi, 0.75, 10^{-3})$. The structure factor $Q_y(k)$ shows a clear peak at $k = 0.5\pi$, corresponding to an oscillation period of four sites. The envelope is well fitted by $A^{\mathrm{LL}}(|j - l|) = 0.33/|j - l|^{0.56}$. We note that this LL-SP phase is also found in the SOC-induced nearest-neighbor spin-flip model and fermionic ladder in gauge field [26–28].

In the following we systematically analyze how the GSs depend on the parameters and give their corresponding phase diagrams. As the system has three independent parameters (ϕ, λ, Ω'), we will concentrate on discussing the phase diagrams in the (λ, Ω') plane for different values of ϕ.

A. $\phi = 0$ or π

We first set the flux to be zero or maximum, i.e., $\phi = 0$ or $\phi = \pi$. In these two limits, the DM interaction is absent, and only the anisotropic Heisenberg coupling and the external field exist. The Hamiltonian is reduced to a(n) (anti)ferromagnetic XXZ model in transverse field,

$$\hat{H}_{\mathrm{eff}} = \mp \frac{1}{\lambda} \sum_j \left[\hat{S}_j^x \hat{S}_{j+1}^x + \hat{S}_j^y \hat{S}_{j+1}^y \pm (2\lambda - 1) \hat{S}_j^z \hat{S}_{j+1}^z \right]$$
$$- \Omega' \sum_j \hat{S}_j^x, \qquad (14)$$

where ferromagnetic coupling corresponds to $\phi = 0$ and antiferromagnetic coupling corresponds to $\phi = \pi$. The phase diagrams of these two models are presented in Figs. 2(a) and 2(b), respectively. We see that due to the absence of DM interaction, the spiral phase is absent, and only (I) the z-FM phase, (II) the x-PM phase, and (III) the y-AFM phase appear. In the following we simply explain the phase transitions between the different phases.

We first consider the ferromagnetic case, i.e., $\phi = 0$. When $\lambda > 1$, the coupling in the $\hat{z}$ direction dominates over that on the $\hat{x}\hat{y}$ plane. The GS is mainly determined by the competition between the coupling in the $\hat{z}$ direction and the transverse field. There is an Ising phase transition as Ω' increases [39]: when Ω' is smaller than a threshold Ω_c', the GS exhibits long-range ferromagnetic correlation along the $\hat{z}$ direction, so is in the z-FM phase; when Ω' increases beyond Ω_c', the z-ferromagnetic correlation vanish completely and the spins are polarized in the $\hat{x}$ direction, thus the GS is in the x-PM phase. The phase boundary between the z-FM and the x-PM phase is determined by M_z, which is nonzero in the z-FM phase and zero in the x-PM phase. In the inset of Fig. 2(a) we plot the long-range correlations M_z and M_x as functions of Ω' at $(\phi, \lambda) = (0, 1.25)$. We observe a phase transition point at
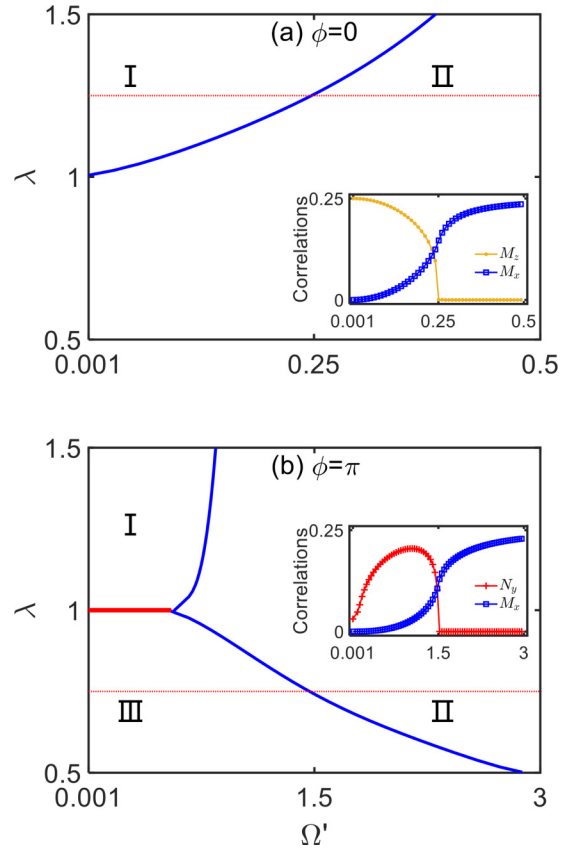

FIG. 2. The GS phase diagrams for (a) $\phi = 0$ and (b) $\phi = \pi$. There are three typical phases with long-range correlations: (I) the z-FM phase, (II) the x-PM phase, and (III) the y-AFM phase. The solid red line in (b) corresponds to a gapless antiferromagnet. The solid blue lines are the phase boundaries. Insets: The long-range correlations as functions of Ω', along (a) $\lambda = 1.25$ and (b) $\lambda = 0.75$, respectively.

$\Omega_c' \approx 0.25$, where M_z drops to zero suddenly as Ω' increases. In fact, the z-FM–x-PM phase transition is not unique for $\phi = 0$, but also applies for an arbitrary value of ϕ when $\lambda > 1$. To avoid repetition we will not refer to it in the following discussions until Sec. III C, where the dependence of this transition on ϕ will be discussed. When $\lambda < 1$, nonzero Ω' breaks the degeneracy of the ferromagnet and polarizes the GS along the $\hat{x}$ direction immediately, as discussed in the weak external field limit. Thus the GS is always in the x-PM phase. We summarize the above analysis in the phase diagram for $\phi = 0$, see Fig. 2(a).

We then consider the antiferromagnetic case, i.e., $\phi = \pi$. When $\lambda = 1$, via rotating every second spin around the $\hat{z}$ axis by an angle π, the Hamiltonian can be transformed into an isotropic ferromagnetic Heisenberg chain in staggered field, that is $\hat{H}_{\mathrm{eff}}' = -\sum_j \vec{S}_j \cdot \vec{S}_{j+1} - \Omega' \sum_j (-1)^j \hat{S}_j^x$. The GS remains a gapless LL phase up to some critical point Ω_c', beyond which it is a fully polarized antiferromagnetic phase [40,41]. They respectively translate to a gapless antiferromagnet and the x-PM phase for our original model. When $\lambda < 1$, the GS is in the twofold degenerate y-AFM phase under weak external fields. In the large external field limit the GS will be in the x-PM phase. There is a finite critical point separating the

y-AFM phase and the x-PM phase. We determine the critical point between the y-AFM and the x-PM phase by the behavior of N_y, which is nonzero in the y-AFM phase and zero in the x-PM phase. In the inset of Fig. 2(b) we plot N_y and M_x as functions of Ω' at $(\phi, \lambda) = (\pi, 0.75)$. We observe that a clear phase transition occurs at $\Omega'_c \approx 1.5$, between the y-AFM phase and the x-PM phase. Our numerical phase diagram for $\phi = \pi$ is shown in Fig. 2(b), which is consistent with the result obtained by mean-field approach if taking care of the definition of parameters [41,42].

B. $\phi = \pi/2$

We then set the flux as $\phi = \pi/2$, at which the anisotropy is absent, and the DM interaction and external field are preserved. The Hamiltonian is reduced to

$$\hat{H}_{\text{eff}} = -\frac{1}{\lambda} \sum_j \left[(2\lambda - 1)\hat{S}_j^z \hat{S}_{j+1}^z + \left(\hat{S}_j^x \hat{S}_{j+1}^y - \hat{S}_j^y \hat{S}_{j+1}^x\right) \right]$$
$$- \Omega' \sum_j \hat{S}_j^x. \quad (15)$$

The phase diagram for $\phi = \pi/2$ is shown in Fig. 3, in which (III) the y-AFM phase is absent, and the two kinds of spiral phases, (IV) the LL-SP phase and (V) the xy-SP phase, emerge. The phase transition between the xy-SP phase and the x-PM phase is characterized by the long-range spiral correlation C_z, which is finite in the xy-SP phase and zero in the x-PM phase. To show this phase transition, we plot C_z and M_x as functions of Ω' along $\lambda = 0.75$ in the inset of Fig. 3. We see that a clear phase transition occurs at $\Omega'_c \approx 0.85$, at which C_z starts to vanish as Ω' increases.

We expect the external field to break the LL-SP phase in the vicinity of $\Omega' = 0$, and lead the GS to the xy-SP phase, which is still of spiral correlation, but with finite spin-spin
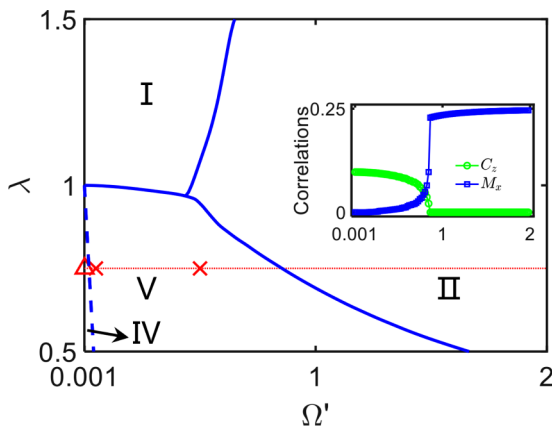

FIG. 3. The GS phase diagrams for $\phi = \pi/2$. There are four different phases: (I) the z-FM phase, (II) the x-PM phase, (IV) the LL-SP phase, and (V) the xy-SP phase. The solid blue lines are the phase boundaries, and the dashed blue line separates the LL-SP phase and the xy-SP phase. The red triangle at $(\lambda, \Omega') = (0.75, 10^{-3})$, and the red crosses at $(0.75, 0.05)$ and $(0.75, 0.5)$ denote the parameter values at which we present the spin-spin correlation functions and structure factors in Figs. 1(c) and 4, respectively. Inset: The long-range correlations as functions of Ω' along $\lambda = 0.75$.

correlations in the long range. We can gain some insights from the analogous case at $\phi = 0$ (π), where a nonzero external field lifts the degeneracy of the gapless ferromagnets (antiferromagnets) and induces long-range paramagnetic (antiferromagnetic) spin-spin correlations, as discussed in the weak external fields limit. We anticipate that this scenario applies to other values of ϕ, and the external field also induces long-range spin-spin correlations. Indeed, the spin-spin correlations in the xy-SP phase do not vanish in the long range. In Fig. 4 we plot $\mathcal{S}_{jl}^x$ and $\mathcal{S}_{jl}^y$ versus $|j - l|$ at relative small and large values of Ω'. When Ω' is weak, $\mathcal{S}_{jl}^x$ and $\mathcal{S}_{jl}^y$ exhibit nearly the same behavior as functions of $|j - l|$. The correlations on the even distance oscillate at a period of four sites, with approximately logarithmic decaying envelopes; however, for the odd distance, the envelopes increase in an approximately linear way. This behavior is well described by the function

$$f_c^{\text{SP}}(|j - l|) = A_e^{\text{SP}}(|j - l|)\cos(0.5\pi|j - l|)$$
$$+ A_o^{\text{SP}}(|j - l|)\sin(0.5\pi|j - l|), \quad (16)$$

in which the envelopes A_e^{SP} and A_o^{SP} satisfy

$$A_{e(o)}^{\text{SP}}(|j - l|) = a_{e(o)} \ln|j - l| + b_{e(o)}|j - l| + c_{e(o)}, \quad (17)$$

where the fitting parameters a_e and b_e are both negative, and a_o and b_o are positive, implying that the spin-spin correlations do not vanish in the long range. In Fig. 4(a) we plot $\mathcal{S}_{jl}^y$ and the structure factor $Q_y(k)$ for the xy-SP phase at a representative parameter point $(\lambda, \Omega') = (0.75, 0.05)$. The structure factor has a clear peak at $k = 0.5\pi$, indicating an oscillation period of four sites. The envelope for the even distance is well fitted by $A_e^{\text{SP}}(|j - l|) = -0.0163 \ln|j - l| - 2.47 \times 10^{-5}|j - l| + 0.1054$, and that for the odd distance by $A_o^{\text{SP}}(|j - l|) = 0.0042 \ln|j - l| + 5.95 \times 10^{-5}|j - l| - 0.0079$. When Ω' is relative large, $\mathcal{S}_{jl}^x$ and $\mathcal{S}_{jl}^y$ oscillate in a cosine manner in the long range:

$$f_{x(y)}^{\text{SP}}(|j - l|) = a_{x(y)}\cos(q_{x(y)}|j - l| + \theta_{x(y)}) + b_{x(y)}, \quad (18)$$

where the wave vectors q_x and q_y correspond to the nonzero peak locations of the corresponding structure factors Q_x and Q_y, respectively, which deviate from ϕ and decrease with Ω'; the constant b_x is related to the height of $Q_x(0)$, which can characterize the degree of polarization in the $\hat{x}$ direction and is mainly decided by the strength of Ω'; the constant b_y is always zero, since there is no preferred polarization in the $\hat{y}$ direction; the amplitudes $a_{x(y)}$ and the initial phase $\theta_{x(y)}$ are all dependent on the system parameters. For the particular parameter point $(\phi, \lambda, \Omega') = (\pi/2, 0.75, 0.5)$, $q_{x(y)} \approx 0.467\pi$, $a_{x(y)} \approx 0.0382\,(0.0326)$, $\theta_{x(y)} \approx -0.0842\,(0.0431)$, and $b_x \approx 0.00886$, see Figs. 4(b) and 4(c). According to the behavior of the spin-spin correlations in the long range, we can give an estimation of the boundary separating the LL-SP phase and the xy-SP phase, see the dashed blue line in Fig. 3.

To further show the difference between the LL-SP phase and the xy-SP phase, we perform the finite-size scaling analysis. For this purpose we calculate spin-spin correlations for the LL-SP phase and the xy-SP phase for different system sizes L. We find that the spin-spin correlations also fulfill the rules Eq. (12), (16), or (18). For small Ω' we can extract the long-range spin-spin correlations $\mathcal{S}^\alpha$ from the amplitudes of $\mathcal{S}_{jl}^\alpha$ at the end of the chain (in our calculations, we choose the
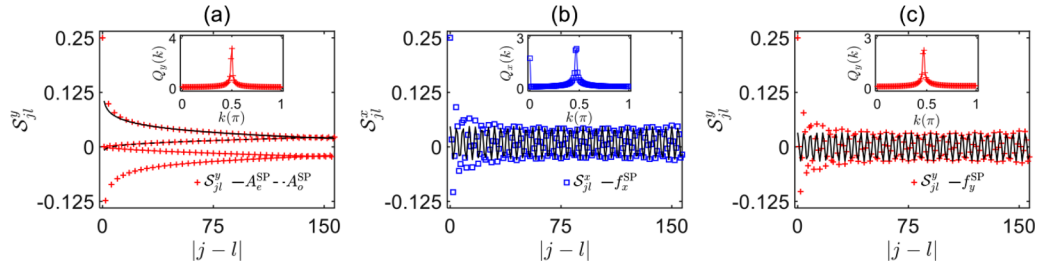
FIG. 4. The spin-spin correlation functions $\mathcal{S}_{jl}^x$ (blue squares) and $\mathcal{S}_{jl}^y$ (red pluses) versus $|j - l|$ for the xy-SP phase at relatively (a) weak strength and (b) and (c) strong strength of the external field. (a) $\mathcal{S}_{jl}^y$ versus $|j - l|$ at $(\phi, \lambda, \Omega') = (0.5\pi, 0.75, 0.05)$. The envelope for the even distance is well fitted by $A_e^{\mathrm{SP}}(|j - l|) = -0.0163 \ln |j - l| - 2.47 \times 10^{-5}|j - l| + 0.1054$ (black solid line), and that for the odd distance by $A_o^{\mathrm{SP}}(|j - l|) = 0.0042 \ln |j - l| + 5.95 \times 10^{-5}|j - l| - 0.0079$ (black dashed line). (b) and (c) $\mathcal{S}_{jl}^x$ and $\mathcal{S}_{jl}^y$ versus $|j - l|$, respectively, at $(\phi, \lambda, \Omega') = (0.5\pi, 0.75, 0.5)$. When $|j - l| > 30$, $\mathcal{S}_{jl}^x$ is well fitted by the function $f_x^{\mathrm{SP}}(|j - l|) = 0.0382 \cos(0.467\pi|j - l| - 0.0842) + 0.00886$ (black line), and $\mathcal{S}_{jl}^y$ is well fitted by the function $f_y^{\mathrm{SP}}(|j - l|) = 0.0326 \cos(0.467\pi|j - l| + 0.0431)$ (black line). Insets: The corresponding spin structure factors $Q_x(k)$ and $Q_y(k)$ versus k.

amplitudes of the fifth oscillation from the bottom to avoid boundary effects). For relatively large Ω', since the spin-spin correlations oscillate in a cosine manner with incommensurate periods, we define $\mathcal{S}^\alpha$ by the maximum value of $\mathcal{S}_{jl}^\alpha$ (in practice, for each L, we only consider $|j - l| \in [L/5, 4L/5]$ to avoid boundary effects). In Fig. 5 we show the finite-size scaling of $\mathcal{S}^\alpha$ for the LL-SP phase, at the representative parameter point $(\phi, \lambda, \Omega') = (\pi/2, 0.75, 10^{-3})$, and the xy-SP phase, at the representative parameter points $(\phi, \lambda, \Omega') = (\pi/2, 0.75, 0.05)$ and $(\pi/2, 0.75, 0.5)$. Through extracting $\mathcal{S}^\alpha$ for different L, it is clear that the long-range spin-spin correlations vanish for the LL-SP phase, but retain finite for the xy-SP phase.

C. ϕ dependence

Finally, we study how the phase transitions depend on the values of ϕ. For this purpose we fix $\lambda = 1.25$ and 0.75, which are chosen to be above and below 1, respectively.

When $\lambda > 1$, for any values of ϕ, the system undergoes the z-FM–x-PM phase transition as Ω' increases. The critical point will increase with ϕ monotonously, as reported
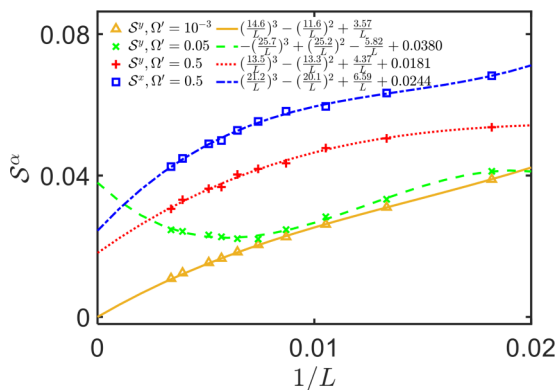

FIG. 5. The finite-size scaling of the long-range spin-spin correlations $\mathcal{S}^\alpha$ for the LL-SP phase at $(\phi, \lambda, \Omega') = (0.5\pi, 0.75, 10^{-3})$ (yellow triangles), and the xy-SP phase at $(\phi, \lambda, \Omega') = (0.5\pi, 0.75, 0.05)$ (green crosses) and $(0.5\pi, 0.75, 0.5)$ (red pluses and blue squares). The marks represent $\mathcal{S}^\alpha$ calculated with system size $L = 55, 75, 95, 115, 135, 155, 175, 195, 255,$ and 295. The lines represent the fittings.

in Fig. 6(a). One can rewrite the Hamiltonian (3) as an Ising model in transverse field plus an isotropic Heisenberg exchange term and a DM interaction term,

$$\hat{H}_{\mathrm{eff}} = -\left(2 - \frac{1 + \cos\phi}{\lambda}\right) \sum_j \hat{S}_j^z \hat{S}_{j+1}^z - \Omega' \sum_j \hat{S}_j^x$$

$$- \frac{1}{\lambda} \sum_j [\cos\phi \mathbf{S}_j \cdot \mathbf{S}_{j+1} + \mathbf{D} \cdot (\mathbf{S}_j \times \mathbf{S}_{j+1})]. \quad (19)$$
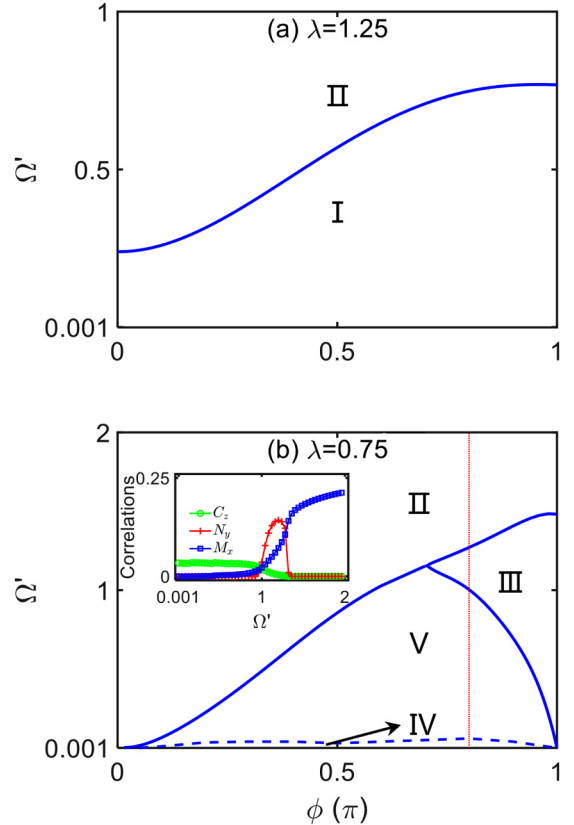

FIG. 6. Flux dependent phase transitions for (a) $\lambda = 1.25$ and (b) $\lambda = 0.75$. (I), (II), (III), (IV), and (V) represent the z-FM phase, the x-PM phase, the y-AFM phase, the LL-SP phase, and the xy-SP phase, respectively. Inset in (b): The long-range correlations as functions of Ω' along $\phi = 0.8\pi$.

Neglecting the last terms and treating the Hamiltonian as an Ising model in the transverse field, which is valid for $\lambda > 1$, one can see that the strength of the coupling in the $\hat{z}$ direction increases with ϕ monotonously, so will the critical points.

When $\lambda < 1$, depending on ϕ, the system may undergo the xy-SP–x-PM, the xy-SP–y-AFM–x-PM, or the y-AFM–x-PM phase transitions as Ω' increases, see Fig. 6(b). When $0 \lesssim \phi < 0.5\pi$, the system always experiences the xy-SP–x-PM phase transition, since the x-x and y-y Heisenberg couplings are ferromagnetic, and only the spiral order and the polarization in the $\hat{x}$ direction may exist. When $\phi = \pi$, the GS undergoes the y-AFM–x-PM phase transition, as studied in Sec. III A. The y-AFM phase exists in a finite range of Ω'. As ϕ deviates from π, we expect the y-AFM phase to not vanish immediately. On the other hand, the GS will be in a spiral phase when $\Omega' \ll 1$. Thus, there should be a phase transition from the spiral phase to the y-AFM phase as Ω' increases. In the inset of Fig. 6(b) we plot the long-range correlations as functions of Ω' for $\phi = 0.8\pi$. As expected, with increasing Ω', first the GS transits from the xy-SP phase to the y-AFM phase at $\Omega' \approx 1$, and then to the x-PM at $\Omega' \approx 1.36$. We note that the phase transition from xy-SP phase to the y-AFM phase is continuous, and the critical point is determined by locating the discontinuous point of the second order derivation of C_z. Of course the y-AFM phase will vanish completely before ϕ reaches 0.5π, since there will be no antiferromagnetic order.

Let us shortly discuss the dependence of the various kinds of critical points on ϕ. When ϕ decreases from π, the critical values of the y-AFM–x-FM phase transition shifts to smaller values of Ω', since the strength of the antiferromagnetic coupling on the $\hat{x}$-$\hat{y}$ plane decreases. At the same time, the critical points between the spiral phase and the y-AFM phase increases, due to the decreasing antiferromagnetic coupling strength and the increasing DM interaction strength. When ϕ increases from zero, the critical value of the xy-SP–x-PM phase transition moves to larger values of Ω', owing to the increasing strength of the DM interaction.

IV. SUMMARY AND DISCUSSIONS

In summary, by employing the MPS method, we have systematically studied the magnetic phase transitions of spin-orbit coupled bosons in 1D optical lattices, which is actually a two-leg ladder with synthetic fluxes. The system can be effectively described by an anisotropic XXZ Heisenberg model with DM interaction and transverse field. Under weak external fields, the GS is the z-FM phase if the ratio of asymmetric interaction strength $\lambda > 1$, and the x-PM phase (around zero flux), the y-AFM phase (around maximum flux), and the LL-SP phase (otherwise) with algebraic decaying spin-spin correlation functions, if $\lambda < 1$. When the transverse field increases, the LL-SP phase will be broken into the xy-SP phase with long-range spin-spin correlations. From the fitting functions of the spin-spin correlation functions and the finite-size scaling in the xy-SP phase, we demonstrate that the spin-spin correlations do not vanish in the long range. From the long-range correlations, we present rich phase diagrams in the parameter spaces.

Interesting extensions of our present study include the magnetic phase transition of the strongly interacting bosons in an artificial three-leg ladder within gauge field, whose single-particle Hamiltonian is realized in [12]. The effective model will be a spin-1 chain, the GS of which would be accessible by the MPS algorithm. In another aspect, in a fermionic synthetic ladder, when taking nuclear spins into consideration, the interorbital spin-exchange interaction [43–45] would couple individual ladders. Thus, model (1) can be generalized to multiple two-leg ladders pierced by an artificial magnetic flux. The impact of this interorbit coupling on the superfluid states has been thoroughly studied in [46]. It induces exotic vortex states on the nuclear-lattice plane, which competes with the existing phases in the decoupled ladder, and leads a rich phase diagram [46]. How this interorbit coupling influences the quantum magnetism in the insulator remains an open question for future research.

APPENDIX A: DERIVATION OF THE EFFECTIVE HAMILTONIAN

We show how to derive our effective Hamiltonian (3) by employing second-order degenerate perturbation theory for quantum system [36]. In the large interacting limit $U, U_{\uparrow\downarrow} \gg t, \Omega$, to obtain the low energy physics, we treat the hopping and on-site spin-flip term $\hat{H}_t$ [Eq. (1)] as perturbation to the on-site interaction term $\hat{H}_U$ [Eq. (2)]. The effective spin model only involves the ground-state subspace of $\hat{H}_U$. With perturbations up to second order, the effective Hamiltonian for the ground-state subspace is given by

$$\hat{H}_{\text{eff}} = \hat{h}_0 + \hat{h}_1 + \hat{h}_2 = E_0 \hat{P}_0 + \hat{P}_0 \hat{H}_t \hat{P}_0 + \hat{P}_0 \hat{H}_t \hat{S} \hat{H}_t \hat{P}_0, \quad \text{(A1)}$$

where $\hat{P}_0$ is the projection operator onto the subspace $\mathcal{U}_0$ spanned by the GSs of $\hat{H}_U$, E_0 is GS energy, and $\hat{S}$ is the projection operator onto the orthogonal complement $\mathcal{V}_0$ of $\mathcal{U}_0$.

At half-filling, i.e., one boson per site, the GSs of the unperturbed Hamiltonian $\hat{H}_U$ are 2^L-fold degenerate with exactly one boson per site with arbitrary spin: $|G_{\vec{\sigma}}\rangle = |\vec{\sigma}\rangle \equiv |\sigma_1 \cdots \sigma_L\rangle$ ($\sigma_i = \uparrow, \downarrow$), with energy $E_0 = 0$. The excited states $|\vec{E}\rangle$ involves multibosons occupying the same site with energy E. The projection operator onto the subspace $\mathcal{U}_0$ reads as

$$\hat{P}_0 = \sum_{\vec{\sigma}} |\vec{\sigma}\rangle\langle\vec{\sigma}|. \quad \text{(A2)}$$

The projection operator onto the orthogonal complement subspace $\mathcal{V}_0$ reads as

$$\hat{S} = \sum_E \frac{1}{E_0 - E} |\vec{E}\rangle\langle\vec{E}|. \tag{A3}$$

The on-site spin-flip term only contributes to $\hat{h}_1$ by coupling two different GSs directly, and the nearest-neighbor hopping term only contributes to $\hat{h}_2$ by coupling two different GSs through a second order virtual process. Thus, the first order perturbation reads as

$$\hat{h}_1 = -\frac{\Omega}{2} \sum_{\vec{\sigma},\vec{\sigma}'} \sum_j \langle\vec{\sigma}|(\hat{a}^\dagger_{j,\uparrow}\hat{a}_{j,\downarrow} + h.c.)|\vec{\sigma}'\rangle|\vec{\sigma}\rangle\langle\vec{\sigma}'|$$

$$= -\frac{\Omega}{2} \sum_j I \otimes \cdots \otimes (|\uparrow\rangle\langle\downarrow| + |\downarrow\rangle\langle\uparrow|)_j \otimes \cdots \otimes I, \tag{A4}$$

where I is a 2×2 identity matrix. The second order perturbation reads as

$$\hat{h}_2 = -\sum_{\vec{\sigma},\vec{\sigma}'} \sum_{j,j'} \sum_E \frac{1}{E} \langle\vec{\sigma}|\hat{T}_{j'}|\vec{E}\rangle\langle\vec{E}|\hat{T}_j|\vec{\sigma}'\rangle|\vec{\sigma}\rangle\langle\vec{\sigma}'|, \tag{A5}$$

where $\hat{T}_j = -t(e^{i\frac{\phi}{2}}\hat{a}^\dagger_{j,\uparrow}\hat{a}_{j+1,\uparrow} + e^{-i\frac{\phi}{2}}\hat{a}^\dagger_{j,\downarrow}\hat{a}_{j+1,\downarrow} + \text{H.c.})$. Obviously for a particular GS $|\vec{\sigma}'\rangle = |\sigma'_1 \cdots \sigma'_L\rangle$, there are only two kinds of excited states that can be coupled to it by $\hat{T}_j$: (i) $|\vec{E}^{\vec{\sigma}'}_{j+1}\rangle = |\sigma'_1 \cdots \sigma'_{j-1}, 0, \sigma'_j\sigma'_{j+1}, \sigma'_{j+2} \cdots \sigma'_L\rangle$, with energy $E^{\vec{\sigma}'}_{j+1} = U\delta_{\sigma'_j,\sigma'_{j+1}} + U_{\uparrow,\downarrow}(1 - \delta_{\sigma'_j,\sigma'_{j+1}})$; (ii) $|\vec{E}^{\vec{\sigma}'}_j\rangle = |\sigma'_1 \cdots \sigma'_{j-1}, \sigma'_j\sigma'_{j+1}, 0, \sigma'_{j+2} \cdots \sigma'_L\rangle$, with energy $E^{\vec{\sigma}'}_j = U\delta_{\sigma'_j,\sigma'_{j+1}} + U_{\uparrow,\downarrow}(1 - \delta_{\sigma'_j,\sigma'_{j+1}})$. The coupling strength reads as

$$\langle\vec{E}|\hat{T}_j|\vec{\sigma}'\rangle = -t\sqrt{1 + \delta_{\sigma'_j,\sigma'_{j+1}}}\left(e^{-\text{sgn}_{\sigma'_j}\frac{i\phi}{2}}\delta_{\vec{E},\vec{E}^{\vec{\sigma}'}_{j+1}} + e^{\text{sgn}_{\sigma'_{j+1}}\frac{i\phi}{2}}\delta_{\vec{E},\vec{E}^{\vec{\sigma}'}_j}\right), \tag{A6}$$

where $\text{sgn}_\uparrow = 1$ and $\text{sgn}_\downarrow = -1$. In turn,

$$\langle\vec{\sigma}|\sum_{j'}\hat{T}_{j'}|\vec{E}^{\vec{\sigma}'}_{j+1}\rangle = -\sqrt{2}t e^{\text{sgn}_{\sigma'_j}\frac{i\phi}{2}}\delta_{\sigma'_j,\sigma'_{j+1}}\delta_{\vec{\sigma}',\vec{\sigma}} - t(1 - \delta_{\sigma'_j,\sigma'_{j+1}})\left(e^{\text{sgn}_{\sigma'_j}\frac{i\phi}{2}}\delta_{\vec{\sigma}',\vec{\sigma}} + e^{\text{sgn}_{\sigma'_{j+1}}\frac{i\phi}{2}}\delta_{\vec{\sigma}'_{(j)},\vec{\sigma}}\right),$$

$$\langle\vec{\sigma}|\sum_{j'}\hat{T}_{j'}|\vec{E}^{\vec{\sigma}'}_j\rangle = -\sqrt{2}t e^{-\text{sgn}_{\sigma'_j}\frac{i\phi}{2}}\delta_{\sigma'_j,\sigma'_{j+1}}\delta_{\vec{\sigma}',\vec{\sigma}} - t(1 - \delta_{\sigma'_j,\sigma'_{j+1}})\left(e^{-\text{sgn}_{\sigma'_{j+1}}\frac{i\phi}{2}}\delta_{\vec{\sigma}',\vec{\sigma}} + e^{-\text{sgn}_{\sigma'_j}\frac{i\phi}{2}}\delta_{\vec{\sigma}'_{(j)},\vec{\sigma}}\right), \tag{A7}$$

where $\vec{\sigma}'_{(j)} = \{\sigma'_1 \cdots \sigma'_{j-1}, \sigma'_{j+1}, \sigma'_j, \sigma'_{j+2} \cdots \sigma'_L\}$, which is defined by exchanging the spin at site j and $j+1$ of the vector $\vec{\sigma}'$. Inserting Eqs. (A6) and (A7) into Eq. (A5) we obtain

$$\hat{h}_2 = t\sum_{\vec{\sigma}',j}\sqrt{1 + \delta_{\sigma'_j,\sigma'_{j+1}}}\left[\frac{e^{-\text{sgn}_{\sigma'_j}\frac{i\phi}{2}}}{E^{\vec{\sigma}'}_{j+1}}\sum_{\vec{\sigma}}\langle\vec{\sigma}|\sum_{j'}\hat{T}_{j'}|\vec{E}^{\vec{\sigma}'}_{j+1}\rangle|\vec{\sigma}\rangle\langle\vec{\sigma}'| + \frac{e^{\text{sgn}_{\sigma'_{j+1}}\frac{i\phi}{2}}}{E^{\vec{\sigma}'}_j}\sum_{\vec{\sigma}}\langle\vec{\sigma}|\sum_{j'}\hat{T}_{j'}|\vec{E}^{\vec{\sigma}'}_j\rangle|\vec{\sigma}\rangle\langle\vec{\sigma}'|\right]$$

$$= -t^2\sum_j\left[\frac{4}{U}I \otimes \cdots \otimes (|\uparrow\uparrow\rangle\langle\uparrow\uparrow| + |\downarrow\downarrow\rangle\langle\downarrow\downarrow|)_{j,j+1} \otimes \cdots \otimes I + \frac{2}{U_{\uparrow\downarrow}}I \otimes \cdots \otimes (|\uparrow\downarrow\rangle\langle\uparrow\downarrow| + |\downarrow\uparrow\rangle\langle\downarrow\uparrow|)_{j,j+1} \otimes \cdots \otimes I\right.$$

$$\left. + \frac{2}{U_{\uparrow\downarrow}}I \otimes \cdots \otimes (e^{-i\phi}|\downarrow\uparrow\rangle\langle\uparrow\downarrow| + e^{i\phi}|\uparrow\downarrow\rangle\langle\downarrow\uparrow|)_{j,j+1} \otimes \cdots \otimes I\right]. \tag{A8}$$

Focusing on the subspace $\mathcal{U}_0$, we introduce the notation $\mathbf{S}_j = \frac{1}{2}\sum_{\alpha,\beta}\hat{a}^\dagger_{j\alpha}\boldsymbol{\sigma}_{\alpha\beta}\hat{a}_{j\beta}$, with $\boldsymbol{\sigma}$ being the Pauli matrices. Inserting this notation into Eqs. (A4) and (A8) and ignoring the constant energy $\propto -\frac{2t^2}{U} - \frac{t^2}{U_{\uparrow\downarrow}}$, we obtain the effective Hamiltonian (3).

We note that for fermions confined in such a 1D optical lattice, the low-energy physics in the Mott insulator can also be described by an effective spin model. For fermions, the on-site interaction only contains interspin ones: $\hat{H}^f_U = U^f_{\uparrow\downarrow}\sum_j \hat{n}_{j\uparrow}\hat{n}_{j\downarrow}$. In the limit $U^f_{\uparrow\downarrow} \gg t, \Omega$ and at the filling of one fermion per site, following the process of the derivation of Eq. (3) and taking care of the commutation relations, we can obtain the effective Hamiltonian:

$$\hat{H}^f_{\text{eff}} = \frac{4t^2}{U^f_{\uparrow\downarrow}}\sum_j\left[\cos\phi(\hat{S}^x_j\hat{S}^x_{j+1} + \hat{S}^y_j\hat{S}^y_{j+1}) + \hat{S}^z_j\hat{S}^z_{j+1}\right.$$

$$\left. + \sin\phi(\hat{S}^x_j\hat{S}^y_{j+1} - \hat{S}^y_j\hat{S}^x_{j+1})\right] - \Omega\sum_j\hat{S}^x_j. \tag{A9}$$

The magnetic phase transition in this model is a transition from the gapless LL phase to the ferromagnetic phase [31].

APPENDIX B: DETAILS OF THE MPS

1. Schmidt decomposition

To express the states of the system as matrix product form, we make use of the Schmidt decomposition (SD). Any pure state on a composite system $\mathcal{H}_A \otimes \mathcal{H}_B$ is read as $|\psi\rangle = \sum_{i_A,i_B}^{N_A,N_B} M_{i_A,i_B}|i_A\rangle|i_B\rangle$, where $|i_A\rangle$ and $|i_B\rangle$ are the bases of subsystems A and B with dimension N_A and N_B, respectively. The SD on $|\psi\rangle$ means it can be decomposed as $|\psi\rangle = \sum_{\alpha=1}^{\chi} S_\alpha|\alpha_A\rangle|\alpha_B\rangle$, where $\{|\alpha_A\rangle\}$ and $\{|\alpha_B\rangle\}$ are the eigenstates of the reduced density matrices $\hat{\rho}_A$ and $\hat{\rho}_B$ of the subsystem A and B, respectively, and S^2_α are their shared eigenvalues, satisfying $\sum_{\alpha=1}^{\chi} S^2_\alpha = 1$, with $\chi = \min(N_A, N_B)$. The set of $\{S_\alpha\}$ are referred to as Schmidt coefficients, and the number of nonzero Schmidt coefficients χ_s, which meets $1 \leqslant \chi_s \leqslant \chi$, is referred to as Schmidt rank. To relate the

SD with the coefficient matrix M, we expand $\{|\alpha_A\rangle\}$ and $\{|\alpha_B\rangle\}$ in the original bases as $|\alpha_A\rangle = \sum_{i_A} U_{i_A,\alpha}|i_A\rangle$ and $|\alpha_B\rangle = \sum_{i_B} V^\dagger_{\alpha,i_B}|i_B\rangle$, with matrices U and V satisfying $U^\dagger U = I$ and $V^\dagger V = I$, where I is the identity matrix of dimension χ. Defining a diagonal matrix S with entries S_α, M can be expanded as $M_{i_A,i_B} = \sum_\alpha U_{i_A,\alpha} S_\alpha V^\dagger_{\alpha,i_B}$, which is just the singular value decomposition (SVD) of the M matrix.

The form of the SD and the hint of the SVD on coefficient matrix M provide an optimal way to approximate the state vector $|\psi\rangle$ with smaller spanned dimension. That is, if the Schmidt coefficients S_α is arranged in a descending order: $S_1 \geqslant S_2 \geqslant \cdots$, and the Schmidt rank is truncated to some smaller $\tilde{\chi} < \chi_s$ by discarding the states with a small-weighted singular value, the state

$$
\begin{aligned}
|\tilde{\psi}\rangle &= \sum_\alpha^{\tilde{\chi}} S_\alpha |\alpha_A\rangle |\alpha_B\rangle \\
&= \sum_{i_A,i_B,\alpha}^{N_A,N_B,\tilde{\chi}} U_{i_A,\alpha} S_\alpha V^\dagger_{\alpha,i_B} |i_A\rangle |i_B\rangle
\end{aligned}
\tag{B1}
$$

is the closest rank-$\tilde{\chi}$ approximation to $|\psi\rangle$ in the sense that the Frobenius norm between the coefficient matrices of these two states is minimized. This property is the key ingredient for the feasibility of MPS algorithm, as can be seen in the following.

2. Matrix product states

Now we show how to represent the quantum states of a system in matrix product form via making use of the SD or SVD. Any pure state in 1D can be written as $|\psi\rangle = \sum_{\sigma_1 \cdots \sigma_L}^d c_{\sigma_1 \cdots \sigma_L}|\sigma_1 \cdots \sigma_L\rangle$, where $\{|\sigma_i\rangle\}$ are the local bases with dimension d, L is the number of lattice sites, and $c_{\sigma_1 \cdots \sigma_L}$ is the complex amplitude. This pure state can be represented as an MPS

$$
\begin{aligned}
|\psi\rangle &= \sum_{\vec{\sigma}} \sum_{a_0 \cdots a_L}^{\chi_0 \cdots \chi_L} A^{\sigma_1[1]}_{a_0,a_1} A^{\sigma_2[2]}_{a_1,a_2} \cdots A^{\sigma_L[L]}_{a_{L-1},a_L}|\vec{\sigma}\rangle \\
&= \sum_{\vec{\sigma}} A^{\sigma_1[1]} A^{\sigma_2[2]} \cdots A^{\sigma_L[L]}|\vec{\sigma}\rangle,
\end{aligned}
\tag{B2}
$$

where $\vec{\sigma}$ is shorted for $\{\sigma_i\}$, following the recursive routine:

$$
\sum_{a_l}^{\chi_l} U_{a_{l-1}\sigma_l,a_l} S_{a_l} V^\dagger_{a_l,\sigma_{l+1}\cdots\sigma_L} = \Psi_{a_{l-1}\sigma_l,\sigma_{l+1}\cdots\sigma_L},
$$

$$
A^{\sigma_l[l]}_{a_{l-1},a_l} = U_{a_{l-1}\sigma_l,a_l},
\tag{B3}
$$

$$
\Psi_{a_l\sigma_{l+1},\sigma_{l+2}\cdots\sigma_L} = (SV^\dagger)_{a_l,\sigma_{l+1}\cdots\sigma_L},
$$

where the initial Ψ is reshaped from the coefficient vector $\Psi_{a_0\sigma_1,\sigma_2\cdots\sigma_L} = c_{\sigma_1\cdots\sigma_L}$ (here $a_0 = 1$ is an auxiliary index), the first equality is the SVD on Ψ, the second equality is just the replacement of matrix U by the tensor $A^{[l]}$, and the last equality is the reshaping of $SV^\dagger$ into a new matrix Ψ. Each $A^{[l]}$ consists of d matrices of bond dimension $\chi_{l-1} \times \chi_l$, which is determined from the SVD: $\chi_l = \min(d^l, d^{L-l})$. The property $U^\dagger U = I$ makes $A^{[l]}$ satisfy the normalization relationship

$$
\sum_{\sigma_l} A^{\sigma_l[l]\dagger} A^{\sigma_l[l]} = I \quad (l < L),
$$

$$
\sum_{\sigma_L} A^{\sigma_L[l]\dagger} A^{\sigma_L[L]} = \langle \psi \mid \psi \rangle.
\tag{B4}
$$

The MPS with all matrices satisfying this normalization condition is called left-canonical MPS. Note that the decomposition of the complex amplitudes is not unique. If the recursive procedure is started from the right side:

$$
\sum_{a_{l-1}}^{\chi_{l-1}} U_{\sigma_1\cdots\sigma_{l-1},a_{l-1}} S_{a_{l-1}} V^\dagger_{a_{l-1},\sigma_l a_l} = \Psi_{\sigma_1\cdots\sigma_{l-1},\sigma_l a_l},
$$

$$
B^{\sigma_l[l]}_{a_{l-1},a_l} = V^\dagger_{a_{l-1},\sigma_l a_l},
\tag{B5}
$$

$$
\Psi_{\sigma_1\cdots\sigma_{l-2},\sigma_{l-1}a_{l-1}} = (US)_{\sigma_1\cdots\sigma_{l-1},a_{l-1}},
$$

where the initial $\Psi_{\sigma_1\cdots\sigma_{L-1},\sigma_L a_L} = c_{\sigma_1\cdots\sigma_L}$ (here $a_L = 1$ is the auxiliary index), the first equality is the SVD on matrix Ψ, the second equality is replacing $V^\dagger$ by tensor $B^{[l]}$, and the last equality is the reshaping of US into a new Ψ, the MPS reads as

$$
\begin{aligned}
|\psi\rangle &= \sum_{\vec{\sigma}} \sum_{a_0 \cdots a_L}^{\chi_0 \cdots \chi_L} B^{\sigma_1[1]}_{a_0,a_1} B^{\sigma_2[2]}_{a_1,a_2} \cdots B^{\sigma_L[L]}_{a_{L-1},a_L}|\vec{\sigma}\rangle \\
&= \sum_{\vec{\sigma}} B^{\sigma_1[1]} B^{\sigma_2[2]} \cdots B^{\sigma_L[L]}|\vec{\sigma}\rangle.
\end{aligned}
\tag{B6}
$$

The tensor $B^{[l]}$ consists of d matrices of bond dimension $\chi_{l-1} \times \chi_l$ and satisfy the normalization condition

$$
\sum_{\sigma_l} B^{\sigma_l[l]} B^{\sigma_l[l]\dagger} = I \quad (l > 1),
$$

$$
\sum_{\sigma_1} B^{\sigma_1[1]} B^{\sigma_1[1]\dagger} = \langle \psi \mid \psi \rangle,
\tag{B7}
$$

making use of the fact $V^\dagger V = I$ on each SVD decomposition. The MPS with all matrices satisfying the above normalization condition is called right-canonical MPS.

In fact, the degree of nonuniqueness is much higher: there is a gauge degree of freedom in writing the MPS. That is, if one inserts an invertible matrix X with dimension $\chi_l \times \chi_l$ and its inverse X^{-1} into two adjacent MPS matrices $M^{\sigma_l[l]}$ and $M^{\sigma_{l+1}[l+1]}$ and makes the transformation $M^{\sigma_l[l]}X \to M^{\sigma_l[l]}, X^{-1}M^{\sigma_{l+1}[l+1]} \to M^{\sigma_{l+1}[l+1]}$, the MPS is invariant. Instructively we can specify a general MPS $|\psi\rangle = \sum_{\vec{\sigma}} M^{\sigma_1[1]} \cdots M^{\sigma_L[L]}|\vec{\sigma}\rangle$ by choosing a site k, which is called the orthogonal center, that all the matrices left and right to it are left- and right-normalized, respectively. This particular kind of MPS is called mixed-canonical MPS. The left- and right-normalization condition can be imposed by the way quite similar to the one constructing MPS from the coefficient vector. The left-normalization condition is imposed by the recursion

$$
\tilde{M}_{a_{l-1}\sigma_l,a_l} = M^{\sigma_l[l]}_{a_{l-1},a_l},
$$

$$
\sum_{a_l'} U^{[L]}_{a_{l-1}\sigma_l,a_l'} S^{[L]}_{a_l'} V^{[L]\dagger}_{a_l',a_l} = \tilde{M}_{a_{l-1}\sigma_l,a_l},
$$

$$
A^{\sigma_l[l]}_{a_{l-1},a_l'} = U^{[L]}_{a_{l-1}\sigma_l,a_l'},
$$

$$
M^{\sigma_{l+1}[l+1]}_{a_l',a_{l+1}} = \sum_{a_l} (S^{[L]}V^{[L]\dagger})_{a_l',a_l} M^{\sigma_{l+1}[l+1]}_{a_l,a_{l+1}},
\tag{B8}
$$

starting from $M^{[1]}$ to $M^{[k]}$. The first equality is the reshaping of tensor $M^{[l]}$ into a matrix $\tilde{M}$, the second equality is the

SVD of $\tilde{M}$, the third equality is the replacement of $U^{[L]}$ by the tensor $A^{[l]}$, and the last equality is the absorption of the matrices $S^{[L]}$ and $V^{[L]\dagger}$ into the next $M^{[l+1]}$. Then the tensors $A^{[l]}$ satisfy the normalization condition Eq. (B4). The bond dimension of each tensor $A^{[l]}$ is determined from the SVD: $\chi'_l = \min(d\chi'_{l-1}, \chi_l)$, where χ_l is the bond dimension of the original tensor $M^{[l]}$. The right-normalization condition is enforced by the recursion

$$\tilde{M}_{a_{l-1},\sigma_l a_l} = M^{\sigma_l[l]}_{a_{l-1},a_l},$$

$$\sum_{a'_{l-1}} U^{[R]}_{a_{l-1},a'_{l-1}} S^{[R]}_{a'_{l-1}} V^{[R]\dagger}_{a'_{l-1},\sigma_l a_l} = \tilde{M}_{a_{l-1},\sigma_l a_l},$$

$$B^{\sigma_l[l]}_{a'_{l-1},a_l} = V^{[R]\dagger}_{a'_{l-1},\sigma_l a_l}, \qquad (B9)$$

$$M^{\sigma_{l-1}[l-1]}_{a_{l-2},a'_{l-1}} = M^{\sigma_{l-1}[l-1]}_{a_{l-2},a_{l-1}} (U^{[R]} S^{[R]})_{a_{l-1},a'_{l-1}},$$

starting from $M^{[L]}$ to $M^{[k]}$. Then the tensors $B^{[l]}$ satisfy the normalization condition Eq. (B7). The bond dimension of each tensor $B^{[l]}$ is determined from the SVD: $\chi'_l = \min(d\chi'_{l+1}, \chi_l)$. At last, multiplying the residual U and S matrices resulting from the two recursion to $M^{[k]}$: $\tilde{M}^{\sigma_k[k]} = (S^{[L]} V^{[L]\dagger}) M^{\sigma_k[k]} (U^{[R]} S^{[R]})$, the mixed-canonical MPS is obtained:

$$|\psi\rangle = \sum_{\vec{\sigma}} A^{\sigma_1[1]} \cdots A^{\sigma_{k-1}[k-1]} \tilde{M}^{\sigma_k[k]} B^{\sigma_{k+1}[k+1]} \cdots B^{\sigma_L[L]} |\vec{\sigma}\rangle. \qquad (B10)$$

The norm square of the state is read as $\langle\psi\mid\psi\rangle = \sum_{\sigma_k} \text{Tr}(\tilde{M}^{\sigma_k[k]\dagger} \tilde{M}^{\sigma_k[k]})$. Definitely, if k is set as 1 or L, the recursion Eq. (B8) or (B9) gives the left- or right-canonical MPS, respectively.

The MPSs obtained in theses ways are exact, but not suitable for numerical computation. This is because the dimension of the matrices grows up exponentially, as can be seen from the recursion constructing the canonical MPS. One way to make the MPSs practicable is to bound the bond dimension to some maximum $\tilde{\chi}$ following Eq. (B1). That is, in the process building a canonical MPS from a state vector or a general MPS, once the bond dimension grows above $\tilde{\chi}$, truncate it to $\tilde{\chi}$ following Eq. (B1). As a result, the elements in the MPS are decimated in block effectively. This approximation is valid for GS in 1D without losing noticeable accuracy, due to two facts: (i) the singular value spectra decay exponentially, and (ii) the bipartite entanglement of the GS obeys an area law in the gapped phase and increases as subsystem size only logarithmically near the critical point. The below MPS algorithm is in fact based on such a decimation procedure.

3. Matrix product operators

The natural generation of writing states as matrix product form to operators is the matrix product operator (MPO). A general operator $\hat{O}$ expressed in the local bases is $\hat{O} = \sum_{\vec{\sigma},\vec{\sigma}'} O_{\vec{\sigma},\vec{\sigma}'} |\vec{\sigma}\rangle\langle\vec{\sigma}'|$. Its matrix product form is defined as

$$\hat{O} = \sum_{\vec{\sigma},\vec{\sigma}'} \sum_{b_1\cdots b_{L-1}}^{D_1\cdots D_{L-1}} W^{\sigma_1,\sigma'_1[1]}_{1,b_1} \cdots W^{\sigma_L,\sigma'_L[L]}_{b_{L-1},1} |\vec{\sigma}\rangle\langle\vec{\sigma}'|$$

$$= \sum_{\{b_l\}} \hat{W}^{[1]}_{1,b_1} \hat{W}^{[2]}_{b_1,b_2} \cdots \hat{W}^{[L]}_{b_{L-1},1}, \qquad (B11)$$

where each $\hat{W}^{[l]}$ can be considered as a $D_{l-1} \times D_l$ operator-valued matrix with elements $\hat{W}^{[l]}_{b_{l-1},b_l} = \sum_{\sigma_l,\sigma'_l} W^{\sigma_l,\sigma'_l[l]}_{b_{l-1},b_l} |\sigma_l\rangle\langle\sigma'_l|$. The expression of the MPO is actually a sum of matrices products, which is of the same form as a general Hamiltonian. This makes it quite intuitive to express a 1D Hamiltonian as an MPO. In fact, through defining some finite state automaton rules, all 1D Hamiltonians with finite-range interaction can be written as exact MPO form [34]. In considering our model Eq. (3), we can write down its MPO representation directly:

$$\hat{W}^{[1]} = \begin{bmatrix} -\Omega'\hat{S}^x & -\frac{1}{\lambda}(\cos\phi\hat{S}^x - \sin\phi\hat{S}^y) & -\frac{1}{\lambda}(\cos\phi\hat{S}^y + \sin\phi\hat{S}^x) & -\frac{2\lambda-1}{\lambda}\hat{S}^z & I \end{bmatrix},$$

$$\hat{W}^{[1<l<L]} = \begin{bmatrix} I & 0 & 0 & 0 & 0 \\ \hat{S}^x & 0 & 0 & 0 & 0 \\ \hat{S}^y & 0 & 0 & 0 & 0 \\ \hat{S}^z & 0 & 0 & 0 & 0 \\ -\Omega'\hat{S}^x & -\frac{1}{\lambda}(\cos\phi\hat{S}^x - \sin\phi\hat{S}^y) & -\frac{1}{\lambda}(\cos\phi\hat{S}^y + \sin\phi\hat{S}^x) & -\frac{2\lambda-1}{\lambda}\hat{S}^z & I \end{bmatrix}, \quad \hat{W}^{[L]} = \begin{bmatrix} I \\ \hat{S}^x \\ \hat{S}^y \\ \hat{S}^z \\ -\Omega'\hat{S}^x \end{bmatrix}. \qquad (B12)$$

4. Variational ground state search

We now show how to obtain the GS using an MPS as a variational ansatze. To find the optimal ground MPS $|\psi\rangle$ with maximum bond dimension χ, we have to minimize the functional

$$\varepsilon[|\psi\rangle] = \langle\psi|\hat{H}|\psi\rangle - E\langle\psi\mid\psi\rangle, \qquad (B13)$$

where E is the Lagrangian multiplier, and $\hat{H}$ is the Hamiltonian in the MPO form. This optimization problem is hard to solve at first glace for the variables appear as products. Fortunately we can get the optimal solution via an iterative algorithm: minimize the energy ε with respect to the tensor $M^{[k]}$ at site k with all other MPS tensors fixed, and obtain the better state lower in energy; move to the next $M^{[k+1]}$ and find the state again lower in energy; repeat sweeping through all sites until the energy is converged, and finally the minimum energy and the corresponding GS are obtained.

To minimize the energy functional ε with respect to a particular $M^{[k]}$, we have to calculate ε explicitly. Suppose the ansatze MPS $|\psi\rangle$ is of mixed-canonical form with the orthogonal center at a chosen k, the overlap can be directly read as $\langle\psi\mid\psi\rangle = \sum_{\sigma_k a_{k-1} a_k} |M^{\sigma_k[k]}_{a_{k-1},a_k}|^2$. The expectation value

of the MPO $\hat{H}$ in $|\psi\rangle$ is written as

$$
\begin{aligned}
\langle\psi|\hat{H}|\psi\rangle = \sum_{\sigma_k,\sigma'_k}\sum_{a_{k-1},a_k}\sum_{a'_{k-1},a'_k}\sum_{b_{k-1},b_k} \\
\times \left(L^{b_{k-1}[k-1]}_{a_{k-1},a'_{k-1}}M^{\sigma_k[k]*}_{a_{k-1},a_k}W^{\sigma_k,\sigma'_k[k]}_{b_{k-1},b_k}M^{\sigma'_k[k]}_{a'_{k-1},a'_k}R^{b_k[k+1]}_{a_k,a'_k}\right),
\end{aligned}
$$

$$(B14)$$

where the tensors L and R are the partial overlap of the Hamiltonian and the state, constructed following the recursive procedure

$$
L^{b_l[l]}_{a_l,a'_l} = \sum_{\sigma_l,\sigma'_l}\sum_{a_{l-1},a'_{l-1}}\sum_{b_{l-1}}L^{b_{l-1}[l-1]}_{a_{l-1},a'_{l-1}}A^{\sigma_l[l]*}_{a_{l-1},a_l}W^{\sigma_l,\sigma'_l[l]}_{b_{l-1},b_l}A^{\sigma'_l[l]}_{a'_{l-1},a'_l},
$$

$$
R^{b_{l-1}[l]}_{a_{l-1},a'_{l-1}} = \sum_{\sigma_l,\sigma'_l}\sum_{a_l,a'_l}\sum_{b_l}B^{\sigma_l[l]*}_{a_{l-1},a_l}W^{\sigma_l,\sigma'_l[l]}_{b_{l-1},b_l}B^{\sigma'_l[l]}_{a'_{l-1},a'_l}R^{b_l[l+1]}_{a_l,a'_l},
$$

$$(B15)$$

with the initial $L^{b_0[0]}_{a_0,a'_0} = R^{b_L[L+1]}_{a_L,a'_L} = 1$. Now take the extremum of Eq. (B13) with respect to $M^{\sigma_k[k]*}_{a_{k-1},a_k}$, we obtain

$$
\sum_{\sigma'_k}\sum_{a'_{k-1},a'_k}\sum_{b_{k-1},b_k}L^{b_{k-1}[k-1]}_{a_{k-1},a'_{k-1}}W^{\sigma_k,\sigma'_k[k]}_{b_{k-1},b_k}R^{b_k[k+1]}_{a_k,a'_k}M^{\sigma'_k[k]}_{a'_{k-1},a'_k}
$$
$$
- EM^{\sigma_k[k]}_{a_{k-1},a_k} = 0. \qquad (B16)
$$

It is an eigenvalue problem $\hat{H}^{[k]}|v^{[k]}\rangle - E|v^{[k]}\rangle = 0$ if we view $M^{[k]}$ as a vector $|v^{[k]}\rangle$ with entries $v^{[k]}_{a_{k-1}\sigma_k a_k} = M^{\sigma_k[k]}_{a_{k-1},a_k}$, and introduce the effective Hamiltonian by the reshaping

$$
\hat{H}^{[k]}_{a_{k-1}\sigma_k a_k, a'_{k-1}\sigma'_k a'_k} = \sum_{b_{k-1},b_k}L^{b_{k-1}[k-1]}_{a_{k-1},a'_{k-1}}W^{\sigma_k,\sigma'_k[k]}_{b_{k-1},b_k}R^{b_k[k+1]}_{a_k,a'_k}. \quad (B17)
$$

Thus the optimal solution $M^{[k]}$ at present can be obtained by solving the effective Hamiltonian $\hat{H}^{[k]}$ for the GS $|v^{[k]}_0\rangle$ with energy E_0 and reshaping $|v^{[k]}_0\rangle$ back to $M^{[k]}$, with E_0 being the current energy.

In summary, the iterative variational GS search algorithm is as follows:

(i) Input. Input $\hat{H}$ in the MPO form, a guessed MPS $|\psi\rangle$ with maximum bond dimension χ, and a tolerance ς for energy convergence.

(ii) Initialization. Transform $|\psi\rangle$ to the right-canonical form according to Eq. (B9). Initialize the 0th tensor $L^{b_0[0]}_{a_0,a'_0} = 1$. Construct all the right overlaps R by Eq. (B15).

(iii) Right sweep. Construct the effective Hamiltonian according to Eq. (B17), solve it for the minimum energy E_0 and state vector $|v^{[k]}\rangle$. Update $M^{[k]}$ by reshaping $M^{\sigma_k[k]}_{a_{k-1},a_k} = v^{[k]}_{a_{k-1}\sigma_k a_k}$. Left-normalize $M^{[k]}$ and move the orthogonal center to the right site $k+1$ by Eq. (B8). Update the kth overlap $L^{[k]}$ recursively following Eq. (B15). Continue sweeping to the right until the boundary is reached.

(iv) Left sweep. Construct the effective Hamiltonian and solve it for the minimum energy E_0 and state vector $|v^{[k]}\rangle$. Update $M^{[k]}$ by reshaping $M^{\sigma_k[k]}_{a_{k-1},a_k} = v^{[k]}_{a_{k-1}\sigma_k a_k}$. Right-normalize $M^{[k]}$ and move the orthogonal center to the left site $k-1$ by Eq. (B9). Update the kth overlap $R^{[k]}$ recursively following Eq. (B15). Continue sweeping to the left until the boundary is reached.

(v) Repeat steps (iii) and (iv) until the convergence is achieved $\langle\hat{H}^2 - E^2_0\rangle < \varsigma$.

(vi) Output. Output the minimum energy E_0 and the MPS $|\psi\rangle$ which is of right-canonical form now.

Note that the state obtained in this way is not necessarily the GS, for it may get stuck in some local minimum state. Two ways help improve such a dilemma. The first is to prepare the initial state in the desired subspace with good quantum number. The approached state must be the energy-minimized state in that subspace. This is not the case for our model, for there is no explicit conserved quantity in our system. The second way is to generalize the single site to a contiguous block during the local search and modify the algorithm accordingly, at the cost of consuming longer computational time and more computational resources.

5. Variational excited states search

With the GS achieved, we now show how to obtain the subsequent excited states incrementally. As the way searching the GS, the nth excited state (nExS) is found by minimizing the energy functional $\varepsilon_n[|\psi_n\rangle] = \langle\psi_n|\hat{H}|\psi_n\rangle - E_n\langle\psi_n\mid\psi_n\rangle$, but under n orthogonality constraints

$$
\langle\psi_n\mid\phi_m\rangle = 0, \qquad (B18)
$$

where $\{|\phi_m\rangle\}$ with $m = 0, 1, \ldots, n-1$ are the n lower-lying eigenstates. It makes the searching program constrained in the space orthogonal to the one formed by $\{|\phi_m\rangle\}$. The minimization of ε_n with respect to local MPS tensor $M^{[k]}$ under such constraints is equivalent to solving the eigenvalue problem

$$
(\hat{P}^{[k]\dagger}\hat{H}^{[k]}\hat{P}^{[k]})|v^{[k]}\rangle - E|v^{[k]}\rangle = 0, \qquad (B19)
$$

where $\hat{H}^{[k]}$, defined by Eq. (B17), is the effective Hamiltonian for the variational local tensor $M^{[k]}$, and $\hat{P}^{[k]}$ is the project operator into the orthogonal space of the lower-lying space $\{|\phi_m\rangle\}$.

To find the projector $\hat{P}^{[k]}$ for every local tensor, we calculate the overlaps between the lower-lying states and the variational state explicitly: $\langle\psi_n\mid\phi_m\rangle = \sum_{a_{k-1},\sigma_k,a_k}M^{\sigma_k[k]*}_{a_{k-1},a_k}F^{\sigma_k[k](m)}_{a_{k-1},a_k}$, with

$$
F^{\sigma_k[k](m)}_{a_{k-1},a_k} = \sum_{a'_{k-1},a'_k}\mathcal{L}^{[k-1](m)}_{a_{k-1},a'_{k-1}}A^{\sigma_k[k](m)}_{a'_{k-1},a'_k}\mathcal{R}^{[k+1](m)}_{a_k,a'_k}, \quad (B20)
$$

where $A^{[k](m)}$ is the kth MPS tensor of the mth lower-lying state, and the tensors $\mathcal{L}^{(m)}$ and $\mathcal{R}^{(m)}$ are the partial overlap between $|\phi_m\rangle$ and $|\psi_n\rangle$, constructed following the recursive procedure

$$
\mathcal{L}^{[l](m)}_{a_l,a'_l} = \sum_{a_{l-1},\sigma_l,a'_{l-1}}M^{\sigma_l[l]*}_{a_{l-1},a_l}\mathcal{L}^{[l-1](m)}_{a_{l-1},a'_{l-1}}A^{\sigma_l[l](m)}_{a'_{l-1},a'_l},
$$

$$
\mathcal{R}^{[l](m)}_{a_{l-1},a'_{l-1}} = \sum_{a_l,\sigma_l,a'_l}M^{\sigma_l[l]*}_{a_{l-1},a_l}\mathcal{R}^{[l+1](m)}_{a_l,a'_l}A^{\sigma_l[l](m)}_{a'_{l-1},a'_l},
$$

$$(B21)$$

with the initial $\mathcal{L}_{a_0,a_0'}^{[0](m)} = 1$ and $\mathcal{R}_{a_L,a_L'}^{[L+1](m)} = 1$. By viewing the tensor $M^{[k]}(F^{[k](m)})$ as vector $|v^{[k]}\rangle(|u^{[k](m)}\rangle)$ with elements $v_{a_{k-1}\sigma_k a_k}^{[k]} = M_{a_{k-1},a_k}^{\sigma_k[k]}$ ($u_{a_{k-1}\sigma_k a_k}^{[k](m)} = F_{a_{k-1},a_k}^{\sigma_k[k](m)}$), the projector $\hat{P}^{[k]}$ for the local tensor space is directly read as

$$\hat{P}^{[k]} = \hat{1} - \sum_{m,m'=0}^{n-1} F^{[k](m)}(\mathcal{N}^{-1})_{mm'} F^{[k](m')\dagger}, \quad (B22)$$

where $(\mathcal{N}^{-1})_{mm'} = \mathrm{Tr}(F^{[k](m)\dagger}F^{[k](m')})$.

The flow of the variational nExS search is the same as that for the GS, but with each step modified accordingly:

(i) Input. Input $\hat{H}$ in the MPO form, the n lower-lying states $\{|\phi_m\rangle\}$ that have already obtained in the MPS form, a guessed MPS $|\psi\rangle$ for the nExS with maximum bond dimension χ, and a tolerance ς for energy convergence.

(ii) Initialization. Transform $|\psi\rangle$ to the right-canonical form according to Eq. (B9). Initialize the 0th tensors $L_{a_0,a_0'}^{b_0[0]} = 1$ and $\mathcal{L}_{a_0,a_0'}^{[0](m)} = 1$. Construct all the right overlaps R and $\mathcal{R}$ by Eqs. (B15) and (B21), respectively.

(iii) Right sweep. Construct the effective Hamiltonian by Eq. (B17) and the projector by Eqs. (B20) and (B22). Solve the projected effective Hamiltonian for the minimum energy E_n and state vector $|v^{[k]}\rangle$. Update $M^{[k]}$ by reshaping $M_{a_{k-1},a_k}^{\sigma_k[k]} = v_{a_{k-1}\sigma_k a_k}^{[k]}$. Left-normalize $M^{[k]}$ and move the orthogonal center to the right site $k+1$ by Eq. (B8). Update the kth overlaps

$L^{[k]}$ and $\mathcal{L}^k$ recursively following Eqs. (B15) and (B21), respectively. Continue sweeping to the right until the boundary is reached.

(iv) Left sweep. Construct the projected effective Hamiltonian and solve it for the minimum energy E_n and state vector $|v^{[k]}\rangle$. Update $M^{[k]}$ by reshaping $M_{a_{k-1},a_k}^{\sigma_k[k]} = v_{a_{k-1}\sigma_k a_k}^{[k]}$. Right-normalize $M^{[k]}$ and move the orthogonal center to the left site $k-1$ by Eq. (B9). Update the kth overlaps $R^{[k]}$ and $\mathcal{R}^{[k]}$ recursively following Eqs. (B15) and (B21), respectively. Continue sweeping to the left until the boundary is reached.

(v) Repeat steps (iii) and (iv) until the convergence is achieved $\langle \hat{H}^2 - E_n^2 \rangle < \varsigma$.

(vi) Output. Output the energy E_n and the MPS $|\psi\rangle$ which is of right-canonical form now.

The variational excited states search also suffers from the local minimum dilemma. Besides, the area law of entanglement does not apply to the bulk excited states, thus the bond dimension χ has to be increased to ensure the discarded states are of small-weighted singular values. This limits the algorithm to be applicable only for low-energy states.

6. Calculation of observables

For a general observable $\hat{O} = \sum_{\vec{\sigma},\vec{\sigma}'} O_{\sigma_1,\sigma_1'}^{[1]} \cdots O_{\sigma_L,\sigma_L'}^{[L]} |\vec{\sigma}\rangle\langle\vec{\sigma}'|$, the expectation value in the state expressed as right-orthogonal MPS is directly written as

$$\langle\hat{O}\rangle = \frac{\sum_{\sigma_L,\sigma_L'} O_{\sigma_L,\sigma_L'}^{[L]} M^{\sigma_L[L]\dagger}\left(\cdots\left(\sum_{\sigma_2,\sigma_2'} O_{\sigma_2,\sigma_2'}^{[2]} M^{\sigma_2[2]\dagger}\left(\sum_{\sigma_1,\sigma_1'} O_{\sigma_1,\sigma_1'}^{[1]} M^{\sigma_1[1]\dagger} M^{\sigma_1'[1]}\right)M^{\sigma_2[2]}\right)\cdots\right)M^{\sigma_L'[L]}}{\sum_{\sigma_1} \mathrm{Tr}(M^{\sigma_1[1]\dagger} M^{\sigma_1[1]})}, \quad (B23)$$

where the dominate is the norm square of the state. When reduced to single-site and two-site cases, the calculation is greatly simplified by making use of the normalization conditions. In calculating the single-site observable $\hat{S}_j^\alpha = \sum_{\sigma_j,\sigma_j'} S_{\sigma_j,\sigma_j'}^{\alpha[j]} |\sigma_j\rangle\langle\sigma_j'|$, it is convenient to transform the right-canonical MPS into one of mixed-canonical form with the orthogonal center at site j. Then the expectation value is just read as

$$\langle\hat{S}_j^\alpha\rangle = \frac{\sum_{\sigma_j,\sigma_j'}\left[S_{\sigma_j,\sigma_j'}^{\alpha[j]} \mathrm{Tr}(M^{\sigma_j[j]\dagger} M^{\sigma_j'[j]})\right]}{\sum_{\sigma_j} \mathrm{Tr}(M^{\sigma_j[j]\dagger} M^{\sigma_j[j]})}. \quad (B24)$$

In calculating the expectation value of the two-site observable $\hat{S}_j^\alpha \hat{S}_l^\beta$ (here we set $j < l$ without lose of generality), we move the orthogonal center k to any site in the range $j \leqslant k \leqslant l$.

The evaluation of the expectation value is thus reduced to contracting the tensors in this range. This can be done in a recursive manner: we first construct a tensor at site j, $G_{a_j,a_j'}^{[j]} = \sum_{\sigma_j,\sigma_j',a_{j-1}} M_{a_{j-1},a_j}^{\sigma_j[j]*} S_{\sigma_j,\sigma_j'}^{\alpha[j]} M_{a_{j-1},a_j'}^{\sigma_j'[j]}$, then generate the next G by the recursion

$$G_{a_m,a_m'}^{[m]} = \sum_{\substack{\sigma_m, a_{m-1} \\ \sigma_m', a_{m-1}'}} G_{a_{m-1},a_{m-1}'}^{[m-1]} M_{a_{m-1},a_m}^{\sigma_m[m]*} O_{\sigma_m,\sigma_m'}^{[m]} M_{a_{m-1}',a_m'}^{\sigma_m'[m]}, \quad (B25)$$

until the lth site is reached, where $O^{[m]}$ is the identity matrix when $m < l$ and $O^{[l]} = S^{\beta[l]}$, and finally the expectation value is calculated as $\langle\hat{S}_j^\alpha \hat{S}_l^\beta\rangle = \frac{\mathrm{Tr}(G^{[l]})}{\mathrm{Tr}(M^{\sigma_k\dagger[k]}M^{\sigma_k[k]})}$.

[1] A. B. Kuklov and B. V. Svistunov, Counterflow Superfluidity of Two-Species Ultracold Atoms in a Commensurate Optical Lattice, Phys. Rev. Lett. **90**, 100401 (2003).

[2] L.-M. Duan, E. Demler, and M. D. Lukin, Controlling Spin Exchange Interactions of Ultracold Atoms in Optical Lattices, Phys. Rev. Lett. **91**, 090402 (2003).

[3] C. Lee, Bose-Einstein Condensation of Particle-Hole Pairs in Ultracold Fermionic Atoms Trapped within Optical Lattices, Phys. Rev. Lett. **93**, 120406 (2004).

[4] V. Galitski and I. B. Spielman, Spin–orbit coupling in quantum gases, Nature (London) **494**, 49 (2013).

[5] H. Zhai, Degenerate quantum gases with spin–orbit coupling: A review, Rep. Prog. Phys. **78**, 026001 (2015).

[6] S. Zhang and G.-B. Jo, Recent advances in spin-orbit coupled quantum gases, J. Phys. Chem. Solids **128**, 75 (2018).

[7] L. Zhang and X. J. Liu, *Spin-Orbit Coupling and Topological Phases for Ultracold Atoms* (World Scientific, 2018), Chap. 1, p. 1.

[8] X.-J. Liu, Z.-X. Liu, and M. Cheng, Manipulating Topological Edge Spins in a One-Dimensional Optical Lattice, Phys. Rev. Lett. **110**, 076401 (2013).

[9] Z. Wu, L. Zhang, W. Sun, X.-T. Xu, B.-Z. Wang, S.-C. Ji, Y. Deng, S. Chen, X.-J. Liu, and J.-W. Pan, Realization of two-dimensional spin-orbit coupling for Bose-Einstein condensates, Science **354**, 83 (2016).

[10] B. Song, L. Zhang, C. He, T. F. J. Poon, E. Hajiyev, S. Zhang, X.-J. Liu, and G.-B. Jo, Observation of symmetry-protected topological band with ultracold fermions, Sci. Adv. **4**, eaao4748 (2018).

[11] A. Celi, P. Massignan, J. Ruseckas, N. Goldman, I. B. Spielman, G. Juzeliūnas, and M. Lewenstein, Synthetic Gauge Fields in Synthetic Dimensions, Phys. Rev. Lett. **112**, 043001 (2014).

[12] B. K. Stuhl, H.-I. Lu, L. M. Aycock, D. Genkina, and I. B. Spielman, Visualizing edge states with an atomic Bose gas in the quantum Hall regime, Science **349**, 1514 (2015).

[13] M. Mancini, G. Pagano, G. Cappellini, L. Livi, M. Rider, J. Catani, C. Sias, P. Zoller, M. Inguscio, M. Dalmonte, and L. Fallani, Observation of chiral edge states with neutral fermions in synthetic Hall ribbons, Science **349**, 1510 (2015).

[14] M. Atala, M. Aidelsburger, M. Lohse, J. T. Barreiro, B. Paredes, and I. Bloch, Observation of chiral currents with ultracold atoms in bosonic ladders, Nat. Phys. **10**, 588 (2014).

[15] M. L. Wall, A. P. Koller, S. Li, X. Zhang, N. R. Cooper, J. Ye, and A. M. Rey, Synthetic Spin-Orbit Coupling in an Optical Lattice Clock, Phys. Rev. Lett. **116**, 035301 (2016).

[16] L. F. Livi, G. Cappellini, M. Diem, L. Franchi, C. Clivati, M. Frittelli, F. Levi, D. Calonico, J. Catani, M. Inguscio, and L. Fallani, Synthetic Dimensions and Spin-Orbit Coupling with an Optical Clock Transition, Phys. Rev. Lett. **117**, 220401 (2016).

[17] S. Kolkowitz, S. L. Bromley, T. Bothwell, M. L. Wall, G. E. Marti, A. P. Koller, X. Zhang, A. M. Rey, and J. Ye, Spin-orbit-coupled fermions in an optical lattice clock, Nature (London) **542**, 66 (2017).

[18] D. Hügel and B. Paredes, Chiral ladders and the edges of quantum Hall insulators, Phys. Rev. A **89**, 023619 (2014).

[19] I. Dzyaloshinsky, A thermodynamic theory of "weak" ferromagnetism of antiferromagnetics, J. Phys. Chem. Solids **4**, 241 (1958).

[20] T. Moriya, Anisotropic superexchange interaction and weak ferromagnetism, Phys. Rev. **120**, 91 (1960).

[21] Z. Cai, X. Zhou, and C. Wu, Magnetic phases of bosons with synthetic spin-orbit coupling in optical lattices, Phys. Rev. A **85**, 061605(R) (2012).

[22] W. S. Cole, S. Zhang, A. Paramekanti, and N. Trivedi, Bose-Hubbard Models with Synthetic Spin-Orbit Coupling: Mott Insulators, Spin Textures, and Superfluidity, Phys. Rev. Lett. **109**, 085302 (2012).

[23] J. Radić, A. Di Ciolo, K. Sun, and V. Galitski, Exotic Quantum Spin Models in Spin-Orbit-Coupled Mott Insulators, Phys. Rev. Lett. **109**, 085303 (2012).

[24] M. Gong, Y. Qian, M. Yan, V. W. Scarola, and C. Zhang, Dzyaloshinskii-Moriya interaction and spiral order in spin-orbit coupled optical lattices, Sci. Rep. **5**, 10050 (2015).

[25] J.-G. Wang, S.-P. Feng, and S.-J. Yang, Variational study of phase diagrams of spin-orbit coupled bosons, New J. Phys. **18**, 103053 (2016).

[26] J. Zhao, S. Hu, J. Chang, F. Zheng, P. Zhang, and X. Wang, Evolution of magnetic structure driven by synthetic spin-orbit coupling in a two-component Bose-Hubbard model, Phys. Rev. B **90**, 085117 (2014).

[27] M. Piraud, Z. Cai, I. P. McCulloch, and U. Schollwöck, Quantum magnetism of bosons with synthetic gauge fields in one-dimensional optical lattices: A density-matrix renormalization-group study, Phys. Rev. A **89**, 063618 (2014).

[28] Z. Xu, W. S. Cole, and S. Zhang, Mott-superfluid transition for spin-orbit-coupled bosons in one-dimensional optical lattices, Phys. Rev. A **89**, 051604(R) (2014).

[29] S. Peotta, L. Mazza, E. Vicari, M. Polini, R. Fazio, and D. Rossini, The XYZ chain with Dzyaloshinsky-Moriya interactions: From spin-orbit-coupled lattice bosons to interacting Kitaev chains, J. Stat. Mech. (2014) P09005.

[30] J. Zhao, S. Hu, J. Chang, P. Zhang, and X. Q. Wang, Ferromagnetism in a two-component Bose-Hubbard model with synthetic spin-orbit coupling, Phys. Rev. A **89**, 043611 (2014).

[31] G. Sun, J. Jaramillo, L. Santos, and T. Vekua, Spin-orbit coupled fermions in ladderlike optical lattices at half filling, Phys. Rev. B **88**, 165101 (2013).

[32] F. Verstraete, V. Murg, and J. I. Cirac, Matrix product states, projected entangled pair states, and variational renormalization group methods for quantum spin systems, Adv. Phys. **57**, 143 (2008).

[33] U. Schollwöck, The density-matrix renormalization group in the age of matrix product states, Ann. Phys. **326**, 96 (2011).

[34] M. L. Wall and L. D. Carr, Out-of-equilibrium dynamics with matrix product states, New J. Phys. **14**, 125015 (2012).

[35] E. Brion, L. H. Pedersen, and K. Mølmer, Adiabatic elimination in a lambda system, J. Phys. A: Math. Theor. **40**, 1033 (2007).

[36] M. Takahashi, Half-filled Hubbard model at low temperature, J. Phys. C: Solid State Phys. **10**, 1289 (1997).

[37] M. Takahashi, *Thermodynamics of One-Dimensional Solvable Models* (Cambridge University Press, Cambridge, 2005).

[38] S. Mori, J.-J. Kim, and I. Harada, Effect of a symmetry-breaking field on the ground state of the spin-1/2 antiferromagnetic linear chain, J. Phys. Soc. Jpn. **64**, 3409 (1995).

[39] L. Barbiero, M. Abad, and A. Recati, Magnetic phase transition in coherently coupled Bose gases in optical lattices, Phys. Rev. A **93**, 033645 (2016).

[40] F. C. Alcaraz and A. L. Malvezzi, Critical and off-critical properties of the XXZ chain in external homogeneous and staggered magnetic fields, J. Phys. A: Math. Gen. **28**, 1521 (1995).

[41] D. V. Dmitriev, V. Ya. Krivnov, A. A. Ovchinnikov, and A. Langari, One-dimensional anisotropic Heisenberg model in the transverse magnetic field, J. Exp. Theor. Phys. **95**, 538 (2002).

[42] D. V. Dmitriev, V. Ya. Krivnov, and A. A. Ovchinnikov, Gap generation in the XXZ model in a transverse magnetic field, Phys. Rev. B **65**, 172409 (2002).

[43] G. Cappellini, M. Mancini, G. Pagano, P. Lombardi, L. Livi, M. Siciliani de Cumis, P. Cancio, M. Pizzocaro, D. Calonico,

F. Levi, C. Sias, J. Catani, M. Inguscio, and L. Fallani, Direct Observation of Coherent Interorbital Spin-Exchange Dynamics, Phys. Rev. Lett. **113**, 120402 (2014).

[44] F. Scazza, C. Hofrichter, M. Höfer, P. C. De Groot, I. Bloch, and S. Fölling, Observation of two-orbital spin-exchange interactions with ultracold SU(N)-symmetric fermions, Nat. Phys. **10**, 779 (2014).

[45] X. Zhang, M. Bishof, S. L. Bromley, C. V. Kraus, M. S. Safronova, P. Zoller, A. M. Rey, and J. Ye, Spectroscopic observation of SU(N)-symmetric interactions in Sr orbital magnetism, Science **345**, 1467 (2014).

[46] X. Zhou, J.-S. Pan, W. Yi, G. Chen, and S. Jia, Interaction-induced exotic vortex states in an optical lattice clock with spin-orbit coupling, Phys. Rev. A **96**, 023627 (2017).